Journal of Oceanography, Vol. 55, pp. 543 to 558. 1999

Short Contribution

A Coastal Air-Ocean Coupled System (CAOCS) Evaluated Using an Airborne Expendable Bathythermograph (AXBT) Data Set

PETER C. CHU[1], SHIHUA LU[2] and YUCHUN CHEN[2]

[1]*Department of Oceanography, Naval Postgraduate School, Monterey, CA 93943, U.S.A.*
[2]*Institute of Plateau Atmospheric Physics, Academia Sinica, Langzhou, China*

(Received 1 December 1998; in revised form 16 February 1999; accepted 5 March 1999)

A coastal atmosphere-ocean coupled system (CAOCS) is developed with Princeton Ocean Model (POM) as the oceanic component, and with National Center for Atmospheric Research (NCAR) regional climate model (RegCM2) as the atmospheric component. The model domain (98.84°–121.16°E, 3.06°S–25.07°N) covers the whole SCS and surrounding land and islands. The surface fluxes of water, heat (excluding solar radiation), and momentum are applied synchronously with opposite signs in the atmosphere and ocean. Flux adjustments are not used. The CAOCS model was verified using an intensive airborne expendable bathythermograph (AXBT) survey between 14–25 May 1995 over the majority of the SCS down to about 300-m depth.

Keywords:
· South China Sea circulation,
· regional climate model,
· Princeton ocean model,
· airborne expandable bathythermograph (AXBT).

1. Introduction

The South China Sea (SCS) is a semi-enclosed tropical sea located between the Asian land mass to the north and west, the Philippine Islands to the east, Borneo to the southeast, and Indonesia to the south (Fig. 1), a total area of 3.5×10^6 km^2. It includes the shallow Gulf of Thailand and connections to the East China Sea (through the Taiwan Strait), the Pacific Ocean (through the Luzon Strait), the Sulu Sea, the Java Sea (through the Gasper and Karimata Straits) and to the Indian Ocean (through the Strait of Malacca). All of these straits are shallow except the Luzon Strait whose maximum depth is 1800 m. Consequently the SCS is considered a semi-enclosed water body (Huang and Wang, 1994). The complex topography includes the broad shallows of the Sunda Shelf in the south/southwest; the continental shelf of the Asian landmass in the north, extending from the Gulf of Tonkin to the Taiwan Strait; a deep, elliptical shaped basin in the center, and numerous reef islands and underwater plateaus scattered throughout. The shelf that extends from the Gulf of Tonkin to the Taiwan Strait is consistently near 70 m deep, and averages 150 km in width; the central deep basin is 1900 km along its major axis (northeast-southwest) and approximately 1100 km along its minor axis, and extends to over 4000 m deep. The Sunda Shelf is the submerged connection between southeast Asia, Malaysia, Sumatra, Java, and Borneo and reaches 100 m depth in the middle; the center of the Gulf of Thailand is about 70 m deep.

The SCS is subjected to a seasonal monsoon system (Wyrtki, 1961). From April to August, the weaker southwesterly summer monsoon winds result in a wind stress of just over 0.1 N/m^2 (Fig. 2(a)). From November to March, the stronger northeasterly winter monsoon winds corresponds to a maximum wind stress of nearly 0.3 N/m^2 (Fig. 2(b)). The transitional periods are marked by highly variable winds and surface currents. A survey by Wyrtki (1961) revealed complex temporal and spatial features of the surface currents in both the SCS and the surrounding waters. By April the northeast monsoon has decayed and the main SCS current consists of two large cyclonic eddies in the western SCS, one in the north and the other in the south (Fig. 3(a)). With the beginning of the southwest monsoon in May and June, a wind drift current is formed. Off the coast of Vietnam westward intensification of this current is clearly visible. The wide, uniform drift in the northern SCS shows a deflection of the current to the right of the wind. A large part of the water passes south of Taiwan and into the root of the Kuroshio. The southern SCS is occupied by an anticyclonic eddy (Fig. 3(b)).

The observed circulation patterns of the intermediate to upper layers of the SCS are primarily forced by the local monsoon systems (Wyrtki, 1961), with contributions from the Kuroshio Current via the Bashi Channel, in the southern half of the Luzon Strait. The Kuroshio enters the SCS through the southern side of the channel then executes a tight, anticyclonic turn and exits the SCS near Taiwan. An

Copyright © The Oceanographic Society of Japan.

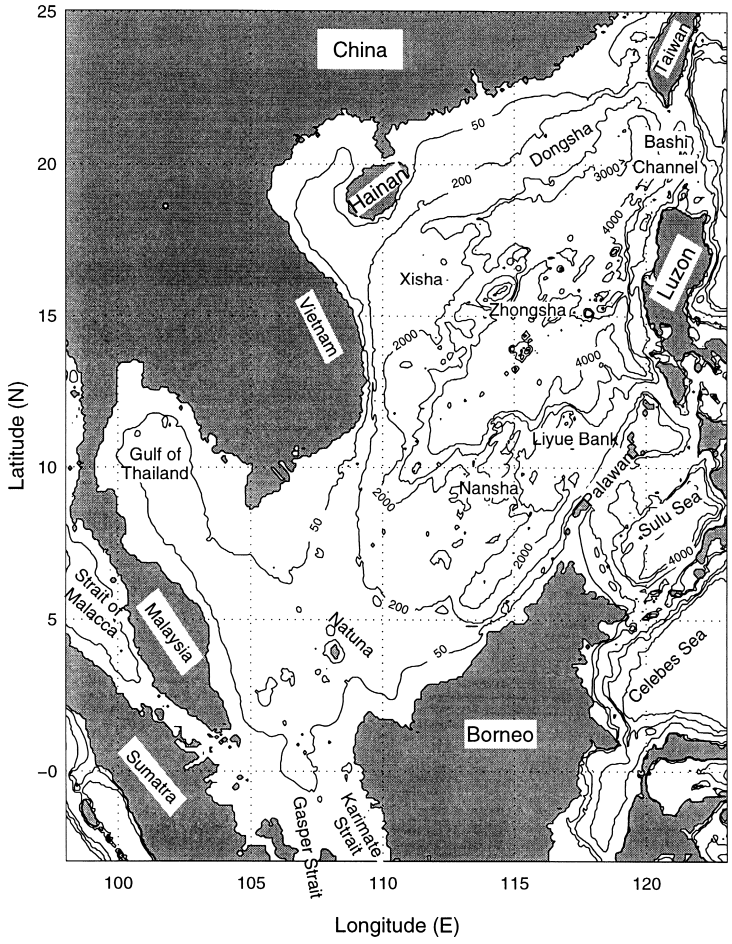

Fig. 1. Geography and isobaths showing the bottom topography of the South China Sea. Numbers show the depth in meter.

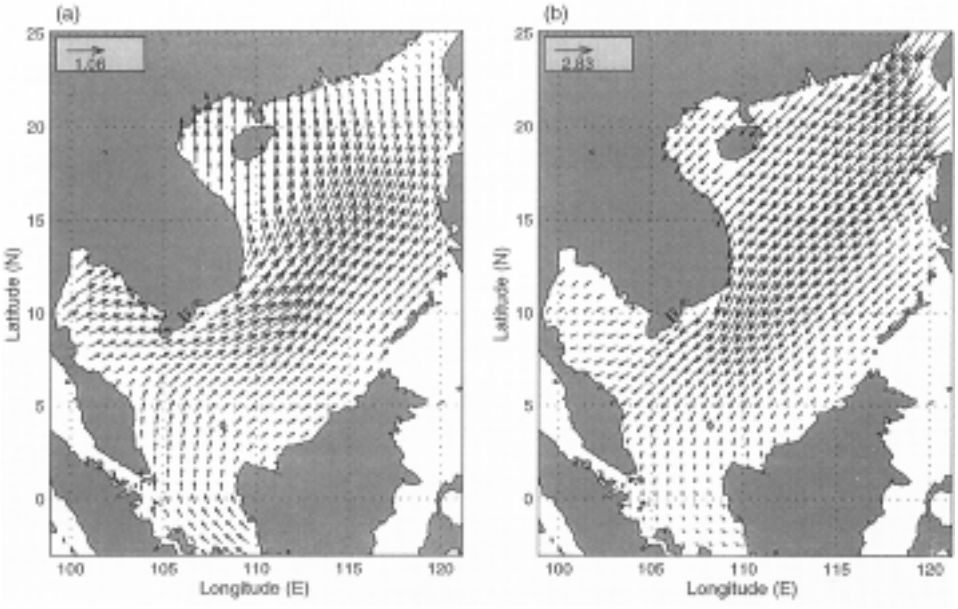

Fig. 2. Climatological wind stress (0.1 N/m^2) for (a) June, and (b) December.

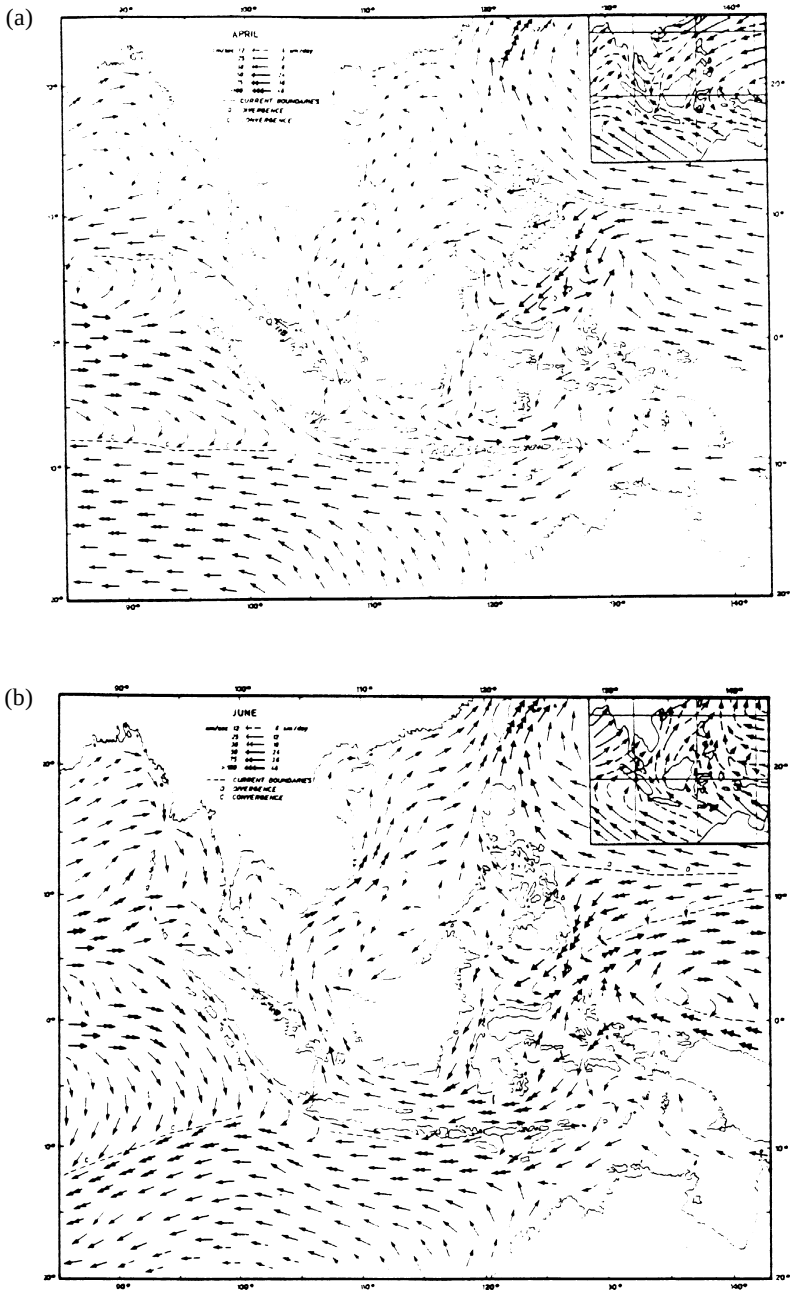

Fig. 3. Observational surface circulation: (a) June, and (b) December (after Wyrtki, 1961).

estimated 8–10 Sv (1 Sv = 10^6 m^3/s) of the intrusion passes through the Bashi Channel (Huang and Wang, 1994). This flow exerts a strong influence on the properties of the northern SCS waters and is believed to contribute to currents in the Taiwan Strait (Hu and Liu, 1992).

Seasonal occurrence of SCS eddies have been reported by several authors. Dale (1956) and Uda and Nakao (1974) reported a cold eddy off the central Vietnam coast in summer. Nitani (1970) found a cold eddy located northwest of Luzon in summer. Reports from the South China Sea Institute of Oceanology (SCSIO, 1985) indicate that a warm-core eddy appears in summer and winter in the central SCS, but closer to Vietnam in summer at the surface. Recently, a cold-core eddy was detected in the central SCS during 29 December 1993 to 5 January 1994 from the analysis of TOPEX/POSEIDON data (Soong *et al.*, 1995). Chu *et al.* (1997a) and Chu and Chang (1997) identified the existence of a central SCS surface warm-core eddy in mid-May from a historical data set—the U.S. Navy's Master Observational Oceanographic Data Set (MOODS). From the composite

analysis on the U.S. National Centers for Environmental Prediction (NCEP) monthly SST fields (1982–1994), Chu *et al*. (1997b) found that during the spring-to-summer monsoon transition (March to May) a warm anomaly (>1.8°C) is formed in the central SCS at 112°–119°30′ E, 15°–19°30′ N.

Understanding the mechanisms of monsoon onset improves the intraseasonal and interannual prediction. An international South China Sea Monsoon Experiment (SCSMEX) was recently initiated to provide a better understanding of the key physical processes for the onset, maintenance and variability of the monsoon over Southeast Asia and southern China leading to improved prediction (SCSMEX Science Working Group, 1995). As one of the SCSMEX modeling efforts, we developed a coastal atmosphere-ocean coupled system (CAOCS) for the South China Sea (SCS) prediction. The oceanic component consists of the Princeton Ocean Model (POM), and the atmospheric component consists of the recent version of the regional climate model (RegCM2) developed at the National Center for Atmospheric Research (NCAR), which is a modified version of the NCAR-Pennsylvania State University Mesoscale Model (MM4) for climate application.

2. An Observational Study on SCS Warm-Core and Cool-Core Eddies

Chu *et al*. (1998a) analyzed the sub-surface thermal

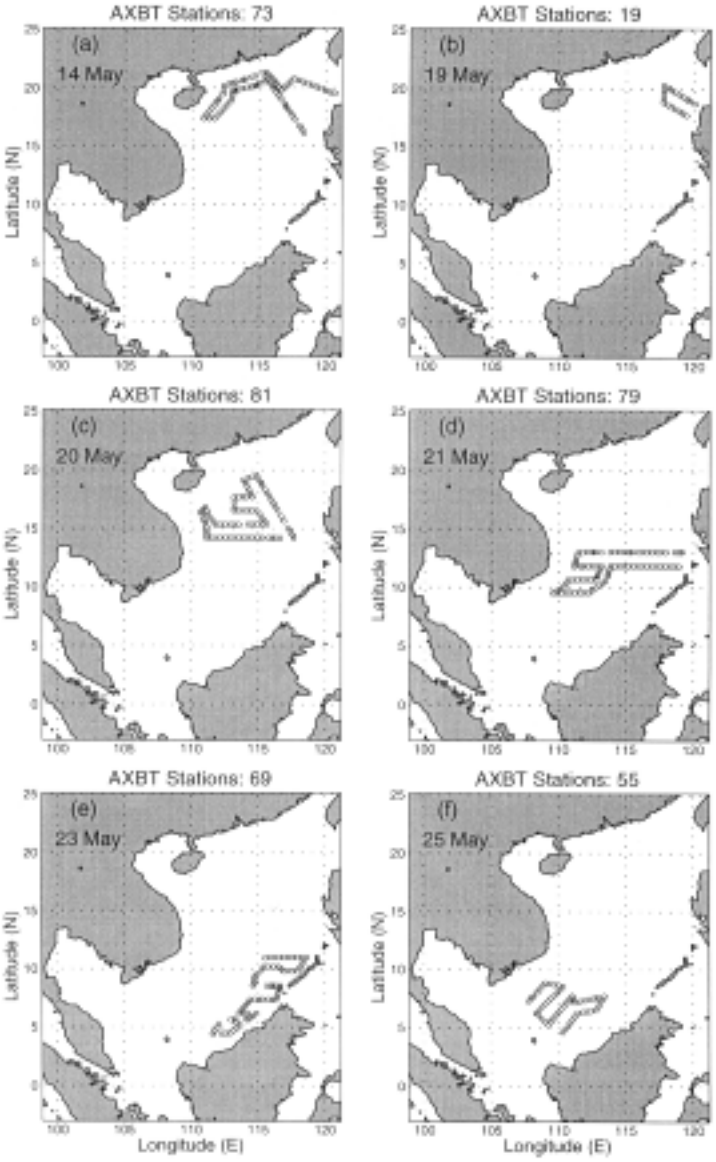

Fig. 4. Deployment pattern of AXBT survey during 14–25 May 1995 (after Chu *et al*., 1998a).

structure and circulation pattern of the SCS eddies from an intensive airborne expendable bathythermograph (AXBT) survey conducted by the Naval Oceanographic Office between 14–25 May 1995 over the majority of the SCS down to about 300-m depth. Figure 4 shows the daily AXBT deployment. This data set provides something close to a "snapshot" of the temperature of the upper ocean in the SCS during the summer monsoon onset.

The AXBT data identified a multi-eddy structure. Figures 5(a)–(e) are horizontal depictions of temperature at 0-, 50-, 100-, 200-, and 300-m depths, respectively. The contour interval is 0.5°C. In them we see that warmer water is situated at the central SCS with surrounding cooler water. At 50-m depth, the 28°C isotherm separates the warm central SCS water from the surrounding cooler water. The maximum temperature of this warm water reaches 29°C. Chu *et al*. (1998a) used the P-vector method to determine the geostrophic velocity. Since there were no salinity (S) observations in SCS during 14–25 May 1995, May climatological salinity data (Levitus, 1984) were interpolated to the AXBT stations and those salinity values ($\overline{S}$) were used for the P-vector computation.

The central SCS warm-core anticyclonic eddy was surrounded by several cool-core and warm-core eddies with

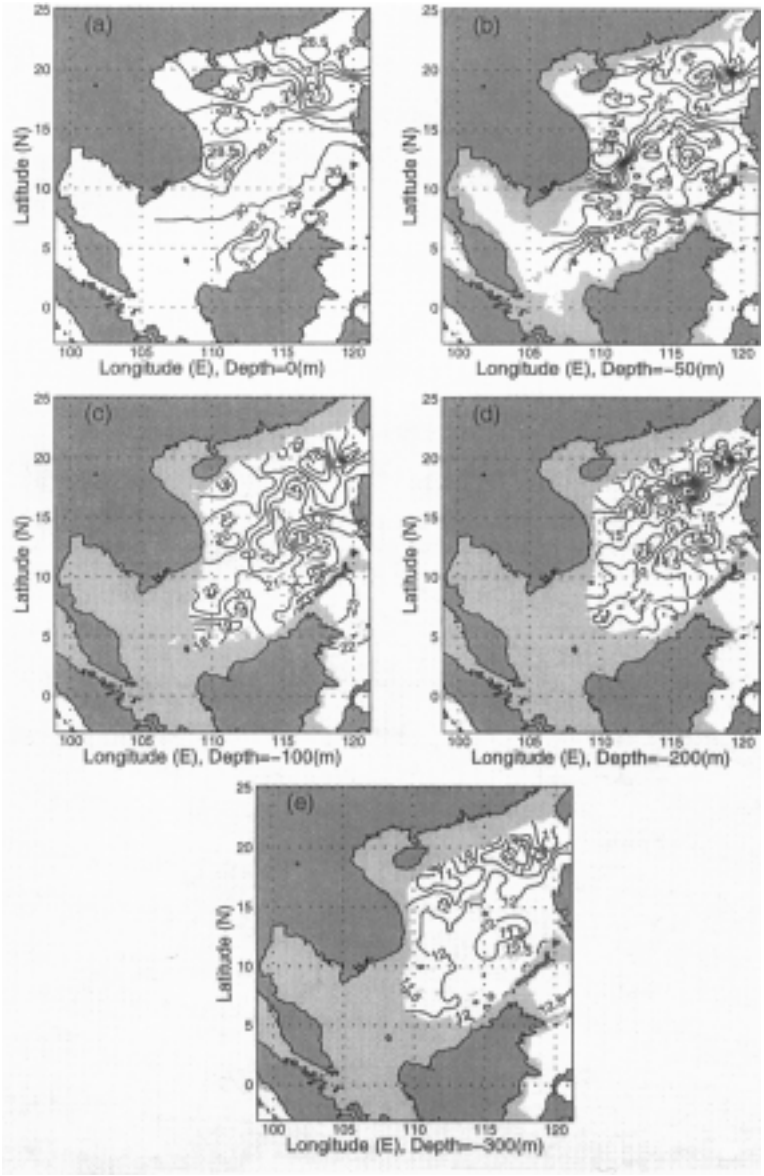

Fig. 5. AXBT measured horizontal temperature fields at different depths: (a) 0-m, (b) 50-m, (c) 100-m, (d) 200-m, and (e) 300-m (after Chu *et al*., 1998a).

a radius of around 100 km and maximum tangential velocities ranging from 10 cm/s to 40 cm/s (Fig. 6). The cool-core eddies were cyclonic and warm-core eddies were anticyclonic. The inverted velocity field shows the existence of: Xisha warm-core anticyclonic eddy with a maximum tangential velocity of 20 cm/s, strongest between the surface and 100-m depth, Dongsha cool-core cyclonic eddy with a maximum tangential velocity of 40 cm/s, strongest between the surface and 200-m depth, South Vietnam cool-core cyclonic eddy between surface and 100-m depth with a maximum tangential velocity of 20 cm/s at surface and decreasing with depth, Liyue cool—core cyclonic eddy with a maximum tangential velocity of 30 cm/s, strongest between the surface and 50-m depth, and Hainan cool-core cyclonic eddy with a maximum tangential velocity of 10 cm/s, the weakest of the cool-core eddies (Fig. 6).

3. CAOCS Model

The CAOCS model was used to simulate the SCS multi-eddy structure in May 1995. The model domain (98.84°–121.16°E, 3.06°S–25.07°N) covers the whole SCS and surrounding land and islands. The integration period in this study is 1–31 May 1995.

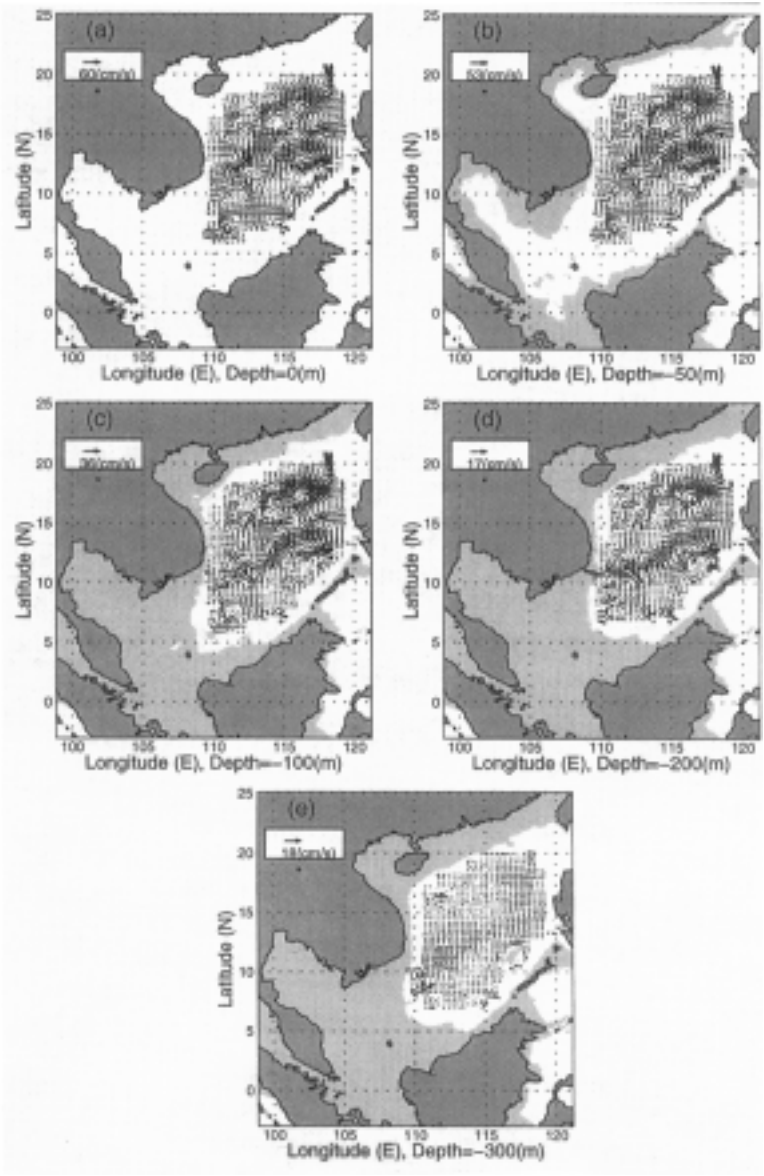

Fig. 6. Geostrophic velocity inverted from the AXBT data by the β-spiral method at different depths: (a) 0-m, (b) 50-m, (c) 100-m, (d) 200-m, and (e) 300-m (after Chu *et al.*, 1998a).

3.1 Ocean component

3.1.1 Model description

We take the Princeton Ocean Model (POM) as the CAOCS ocean component. POM is a time dependent, primitive equation circulation model on a three dimensional grid that includes realistic topography and a free surface. Developed at Princeton University (Blumberg and Mellor, 1987), the model was specifically designed to accommodate mesoscale phenomena, including the often non-linear processes (such as upwelling and eddy dynamics) commonly found in estuarine and coastal oceanography. Tidal forcing was not included in this application of the model, since high frequency variability of the circulation is not considered. River outflow is also not included. However, the seasonal variation in sea surface height, temperature, salinity, circulation and transport are well represented by the model data. From a series of numerical experiments, the qualitative and quantitative effects of non-linearity, wind forcing and lateral boundary transport on the SCS are analyzed, yielding considerable insight into the external factors affecting the regional oceanography.

In this study, we use a rectilinear grid with horizontal spacing of 0.179° by 0.175° (approximately 20 km resolution) and 23 nonuniform vertical σ levels (Table 1). The model uses realistic bathymetry data from the Naval Oceanographic Office Digital Bathymetry Data Base with 5 minute resolution (DBDB5). Consequently, the ocean model contains $125 \times 162 \times 23$ horizontally fixed grid points. The horizontal diffusivities are modeled using the Smagorinsky (1963) form with the coefficient chosen to be 0.2 for this application. The drag coefficient for the bottom stress is specified as 0.0025 (Blumberg and Mellor, 1987; Chu *et al*., 1998c) in our model.

Table 1. Nonhomgeneous σ levels.

σ level	σ value	σ level	σ value	σ level	σ value
1	0	9	–0.3	17	–0.7
2	–0.0125	10	–0.35	18	–0.75
3	–0.025	11	–0.4	19	–0.8
4	–0.5	12	–0.45	20	–0.85
5	–0.1	13	–0.5	21	–0.9
6	–0.15	14	–0.55	22	–0.95
7	–0.2	15	–0.6	23	–1
8	–0.25	16	–0.65		

3.1.2 Lateral boundary conditions

Closed lateral boundaries, i.e., the modeled ocean bordered by land, were defined using a free slip condition for velocity and a zero gradient condition for temperature and salinity. No advective or diffusive heat, salt or velocity fluxes occur through these boundaries. Volume transport through the Luzon Strait, Taiwan Strait, and Gasper/Karimata Strait was defined according to observations (Wyrtki, 1961), as listed in Table 2. The Balabac Channel, Mindoro Strait, and Strait of Malacca are assumed to have zero transport.

Temperature and salinity are likewise prescribed from data when the transport flows into the model domain. When flow is out of the domain, the advection gradient equation is solved for both barotropic and baroclinic modes where the subscript n is the coordinate normal to the boundary (Blumberg and Mellor, 1987).

3.1.3 Initial conditions and initialization

Before coupling to the atmospheric model that is RegCM2, the POM model was integrated for four years and four months from zero velocity, and January climatological temperature and salinity fields (Levitus, 1984) and forced by monthly mean surface wind stress from the Comprehensive Ocean and Atmosphere Data Set (COADS) and by the restoring-type surface heat and salinity fluxes (Haney, 1971) which are relaxed to the surface monthly values. The final states of temperature, salinity, and velocity were taken as the initial ocean conditions for 1 May 1995.

3.2 Atmospheric component

3.2.1 Model description

We take a second generation version of the regional climate model, called RegCM2, as the atmospheric component for CAOCS. RegCM2 is a modified version of the NCAR/Pennsylvania State University mesoscale model MM4 for climate application. The dynamic structure of RegCM2 is essentially the same as MM4 (Anthes *et al*., 1987) that is σ-coordinate, primitive equation, grid point limited-area model with compressibility and hydrostatic balance, except for a split-explicit time integration scheme which is used in RegCM2 to improve model efficiency. The radiative transfer package is from the CCM3 and describes the radia-

Table 2. Bi-monthly variation of volume transport (Sv) at the lateral open boundaries. The positive/negative values mean outflow/inflow and were taken from Wyrtki (1961).

Month	Feb.	Apr.	Jun.	Aug.	Oct.	Dec.
Gaspar-Karimata Straits	4.4	0.0	–4.0	–3.0	1.0	4.3
Luzon Strait	–3.5	0.0	3.0	2.5	–0.6	–3.4
Taiwan Strait	–0.9	0.0	1.0	0.5	–0.4	–0.9

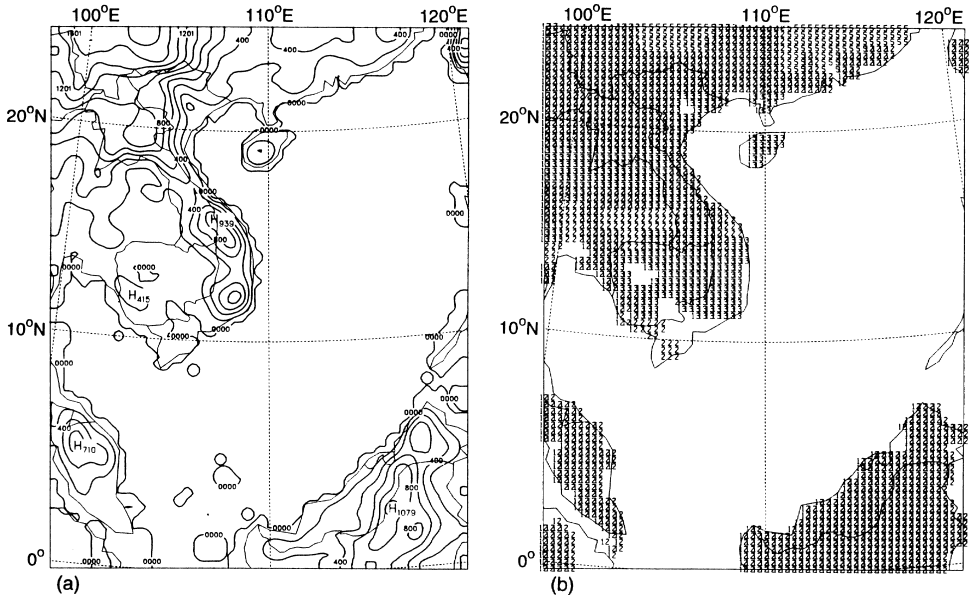

Fig. 7. Surface conditions for the atmospheric component (RegCM2): (a) topography, numbers show the height in meter; and (b) vegetation type (1: urban land, 2: agricultural land, 3: range/grass land, 4: deciduous forest, 5: coniferous forest, 6: mixed forest including wetland, 7: water, 8: non-forest marsh or wetland, 9: desert, and 10: tundra). The 7th type is not marked in the figure.

tive effects of ozone, water vapor, carbon dioxide, oxygen and clouds (Briegleb, 1992). The non-local eddy diffusion formulation of Holtslag *et al*. (1990) is used for planetary boundary layer calculation. The surface process is parameterized by the latest version of the Biosphere-Atmosphere Transfer Scheme (BATS), which describes the effect of vegetation and interactive soil moisture on the surface-atmosphere exchange of momentum, heat, and moisture (Dickinson *et al*., 1993). BATS comprises a vegetation layer, a snow layer, and three soil layers and it calculates the full surface hydrological cycle. The precipitation is parameterized by several different schemes. Non-convective precipitation can be represented via an implicit scheme, whereby supersaturated water immediately precipitates, and an explicit scheme including prognostic equations for cloud water and rain water (Hsie *et al*., 1984). Convective precipitation is parameterized via two cumulus convection schemes: a simplified Kuo-type (Kuo, 1974) formulation and a mass flux scheme which accounts for the effects of penetrative downdrafts (Grell, 1993). The readers are referred to Giorgi *et al*. (1993a, b) for complete description of RegCM2.

3.2.2 Surface parameterization

Figure 7 depicts the topography and vegetation type for the selected domain. The horizontal resolution is 40 km. Sixteen pressure levels were used with the top at 10 mb. The topography data (30′ resolution) were obtained from NCAR. At the present horizontal resolution, we can identify the basic features of the coastlines and some isolated mountains in southeast Asian continent as well as in islands such as Borneo (Fig. 7(a)). A soil water availability function was used for computing the soil water content by using 10 specified vegetation types (Giorgi and Bates, 1989). Figure 7(b) shows the initial vegetation types with the sea surface as the 7th type. Dominant deciduous and coniferous forests cover the most land areas. There are small areas of tropical forest in Taiwan, and Indo-china Peninsula.

3.2.3 Initial and lateral boundary conditions

The initial and horizontal lateral boundary conditions for wind, temperature, water vapor, and surface pressure are interpolated from analyses of observations from European Center for Medium-Range Weather Forecasts (ECMWF). For the present study, they were projected on a spectral T42 grid, and a vertical resolution of 14 pressure levels. The initial conditions were the fields on 00Z May 1, 1995. The lateral boundary conditions were provided via a relaxation method (Anthes *et al*., 1987) and updated every 12 hours.

3.3 Ocean-atmosphere coupling

Atmospheric and oceanic surface fluxes of water, heat (excluding solar radiation), and momentum are of opposite sign and are applied synchronously. Flux adjustments are not used. We use the same flux parameterization as the RegCM2 model for CAOCS. The only difference between the two is the use of sea surface temperature (SST) data. In stand-alone RegCM2 model, SST is prescribed as a given parameter. However, in the CAOCS, SST is predicted by the POM model at each time step for the atmospheric component (RegCM2.)

3.4 Model verification

The simulated atmospheric and oceanic features during the SCS summer monsoon onset were compared to the ECMWF analyzed data, including wind, precipitation, and surface air temperature and the AXBT data. The difference of the simulated and observed of any variable ψ is a function of space (x, y, σ), and time t,

$$\Delta\psi(x_i, y_j, \sigma_k, t) = \psi_s(x_i, y_j, \sigma_k, t) - \psi_o(x_i, y_j, \sigma_k, t),$$

where ψ_s and ψ_o are the variables from simulation and observation, respectively. We define two parameters, the bias and the root-mean-square error (*RMSE*),

$$BIAS = \frac{1}{M}\sum_i\sum_j \Delta\Psi\left(x_i, y_j, \sigma_k, t\right),$$

$$RMSE_\psi\left(\sigma_k, t\right) = \sqrt{\frac{1}{M}\sum_i\sum_j \left|\Delta\Psi\left(x_i, y_j, \sigma_k, t\right)\right|^2} \qquad (1)$$

to evaluate the model performance at level σ_k. Here M is the total number of horizontal points.

4. Simulated SCS Upper Layer Multi-Eddy Structure in May 1995

We integrated the CAOCS for a month from 1 May 1995. The ocean model may still be under adjustment

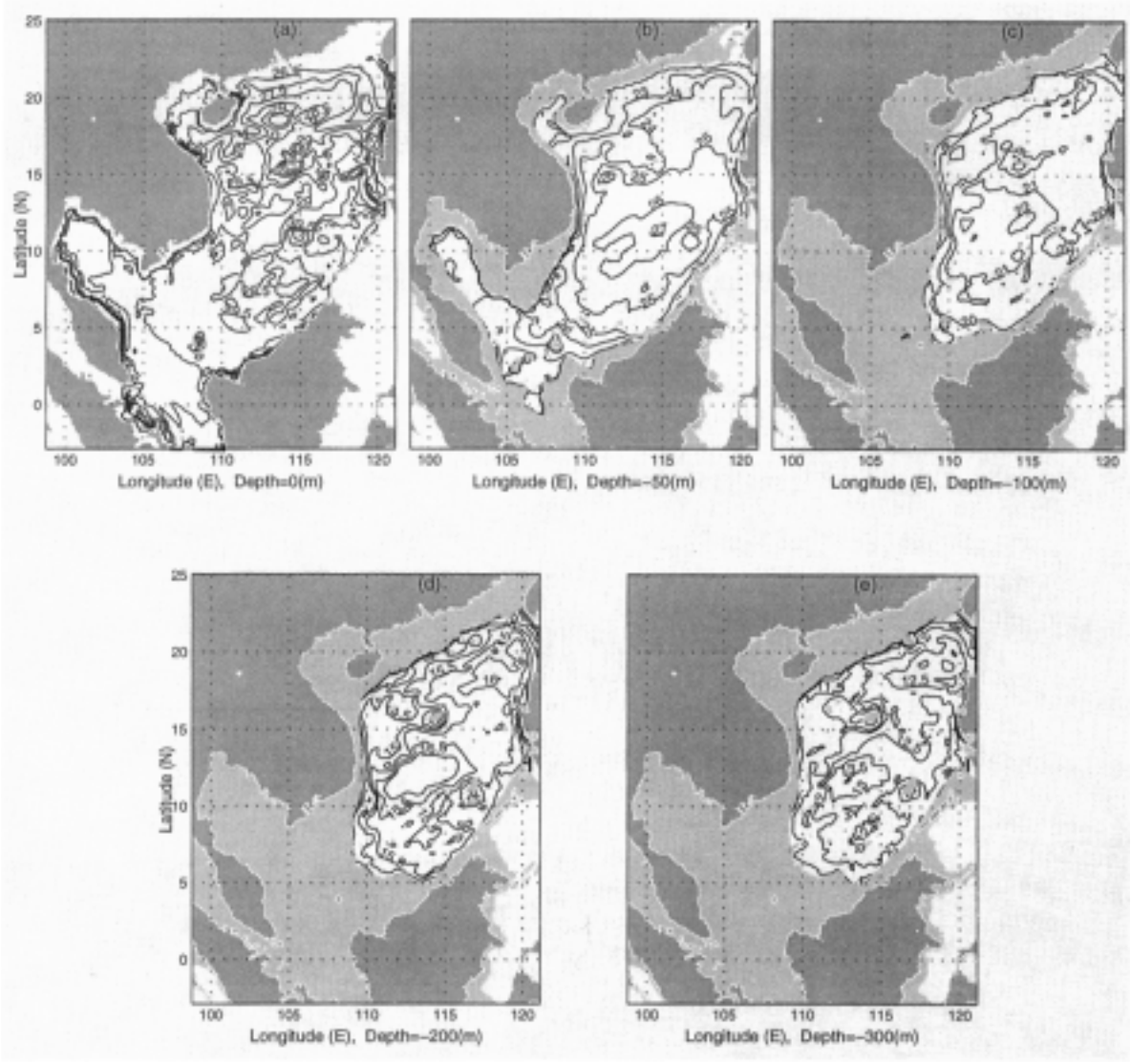

Fig. 8. CAOCS simulated mean horizontal temperature field during 14–25 May 1995 at different depths: (a) 0-m, (b) 50-m, (c) 100-m, (d) 200-m, and (e) 300-m.

processes to the inconsistency at the initial time when the atmospheric and the oceanic models are coupled. However, we are only interested in the SCS upper layer (300 m depth) features. The adjustment time for a shallow layer might be much shorter. The model output is analyzed as follows.

4.1 Thermal structure

To compare the CAOCS model results with the AXBT measurements in May 1995, we present here the time-averaged temperature and velocity fields over 14–25 May 1995.

4.1.1 Horizontal structures

Figures 8(a)–(e) are horizontal depictions of the ocean temperature field from the CAOCS model output at 0-, 50-, 100-, 200-, and 300-m depths, respectively. The contour interval is 0.5°C. Similar to observations, the simulated three dimensional temperature field indicates that warmer water is situated at the central SCS with surrounding cooler water near Zhongsha, Liyue Bank, and South Vietnam. Two weaker warm-core eddies near Xisha and the Bashi Channel are also simulated. At 50-m depth, the simulated central SCS warm-core eddy is located at 112°–117°E, 12°–14°N with a maximum temperature of 27°C (Fig. 8(b)). The location and thermal features of these warm and cool pools are listed in Table 3.

4.1.2 Vertical structures

Four zonal cross-sections (19°N, 17°N, 13°N, and 7°N) of temperature show the vertical structure of the mixed layer and the thermocline as well as the warm and cool pools (Fig. 9). In the 13°N cross-section, the mixed layer deepens at 115°E. The trough and ridge of the isotherms may be considered centers of warm and cool pools.

The 19°N cross-section clearly shows the existence of Bashi warm pool near 117°E from the downward bending (trough) of isotherms. The trough is located at 117°E near 50-m depth, eastward shifted with depth, and kept at 118°E below the 100-m depth. The longitudinal span of central SCS warm pool is around 4°.

The two cross-sections at 17°N and 13°N show the occurrence of central SCS warm pool from the downward bending (trough) of isotherms: 115°E at the 17°N and 114°E at the 13°N. The longitudinal span of central SCS warm pool is around 5° for both latitudes.

The 7°N cross-section shows the eastward uplift of the

Table 3. Locations, typical temperatures, and tangential velocities of the CAOCS simulated SCS warm-core and cool-core eddies during 14–25 May 1995.

Depth (m)	0	50	100	200	300
Central SCS warm-core, Anticyclonic eddy	112°-116°30'E 10°30'-15°N 29°-30°C 20 cm/s	112°-116°30'E 10°30'-15°N 26°-27°C 20 cm/s	112°-116°30'E 11°-15°N 22°C 15 cm/s	113°-116°30'E 11°-14°N 17°C 10 cm/s	114°-117°E 11°30'-14°N 12.5°C 5 cm/s
Bashi warm-core anticyclonic eddy	113°-120°30'E 17°30'-22°N 28.5°C 20 cm/s	113°-120°30'E 17°30'-22°N 24°C 20 cm/s	113°30'-120°30'E 17°30'-21°30'N 21°C 15 cm/s	114°-120°30'E 17°30'-21°30'N 16°C 10 cm/s	114°-120°30'E 17°30'-21°30'N 12.5°C 10 cm/s
Xisha warm-core anticyclonic eddy	109°-113°E 14°-17°N 29.5°C 15 cm/s	109°-113°E 14°-17°N 26°C 15 cm/s	109°-113°E 14°-17°N 21°C 15 cm/s	109°-113°E 14°-17°N 14.5°C 10 cm/s	109°-113°E 14°-17°N 11.5°C 10 cm/s
Liyue cool-core cyclonic eddy	115°30'-117°30'E 9°30'-12°N 29.5°C 20 cm/s	115°30'-117°30'E 9°30'-12°N 25°C 20 cm/s	116°-118°E 10°-12°N 20°C 10 cm/s	116°-118°E 10°-12°N 15°C 10 cm/s	116°-118°30'E 10°-12°30'N 11.5°C 5 cm/s
Luzon cool-core cyclonic eddy	116°-118°30'E 13°-17°N 29.0°C 15 cm/s	116°-118°30'E 12°30'-17°N 25°C 15 cm/s	116°-118°30'E 12°30'-17°N 20°C 15 cm/s	116°-119°E 12°30'-17°N 16°C 15 cm/s	116°-119°E 13°-17°N 12.5°C 10 cm/s
South Vietnam cool-core cyclonic eddy	110°30'-113°E 11°30'-14°N 28°C 20 cm/s	110°30'-113°E 11°30'-14°N 26°C 20 cm/s	110°30'-113°E 11°30'-14°N 19°C 20 cm/s	110°-113°E 11°-14°N 15°C 10 cm/s	109°30'-114°E 10°-14°N 12.5°C 5 cm/s
Zhongsha cool-core cyclonic eddy	112°-115°30'E 14°-17°30'N 29.5°C 16 cm/s	112°-115°30'E 14°-17°30'N 25°C 16 cm/s	112°-115°30'E 14°-17°30'N 19°C 15 cm/s	112°-115°30'E 14°30'-17°30'N 14.5°C 15 cm/s	112°-115°30'E 15°-18°N 11.5°C 10 cm/s

thermocline depth from 50 m at 110°E to 25 m at 115°E. A surface warm pool with SST higher than 29°C was found between 108°–115°E, and a mid-level (100-m) cool pool was detected between 112°–114°E. In the eastern part (114–115°E) an isolated warm pool appeared below the 100-m depth level.

Three latitudinal cross-sections (111°E, 114°E, and 117°E) of temperature also show the vertical structure of the mixed layer and the thermocline as well as the warm and cool pools (Fig. 10). The mixed layer had a shallow-deep-shallow pattern in the latitudinal direction. Taking the 114°E cross-section as an example, the mixed layer had a shallow depth (~20 m) near 5°N. Its depth increased with latitude to about 50-m at 14°N, and decreased with latitude to 20 m near 20°N.

The "trough" and "ridge" of the isotherms may be considered as centers of warm and cool pools. The three cross-sections indicated the occurrence of central SCS warm eddy evident from the downward bending (trough) of isotherms: 9°N at 111°E, 13°N at 114° E, and 15°N and 17°N at 117°E.

4.1.3 Error estimation

We computed both *RMSE* and *BIAS* between the CAOCS modeled ocean temperature field and AXBT data (Fig. 11). The *RMSE* is 0.50°C at the surface, increases with depth to a maximum value of 0.97°C at 20 m, and then reduces with depth to a minimum value of 0.36°C at 300 m. The mean *RMSE* is around 0.6°C (Fig. 11(a)). Besides, the CAOCS modeled SCS temperature is 0.37°C warmer in the upper layer (0–100 m) and 0.31°C cooler in the lower layer (100–300 m) than the AXBT measurement. The highest bias (+0.91°C) appears at 20 m depth (Fig. 11(b)).

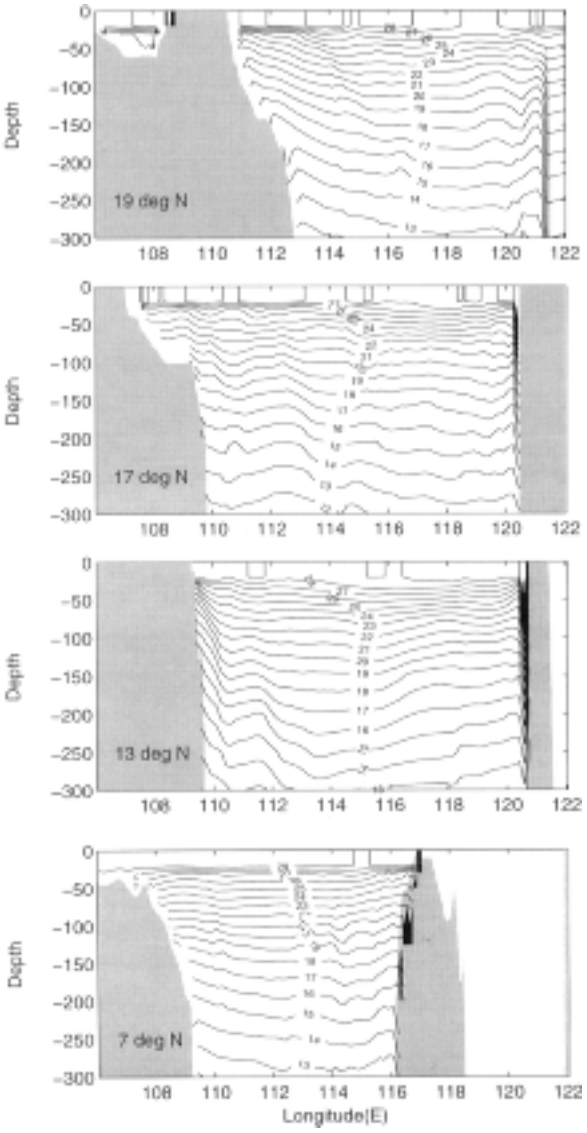

Fig. 9. CAOCS simulated mean temperature field during 14–25 May 1995 at several zonal cross section: (a) 19°N, (b) 17°N, (c) 13°N, and (d) 7°N.

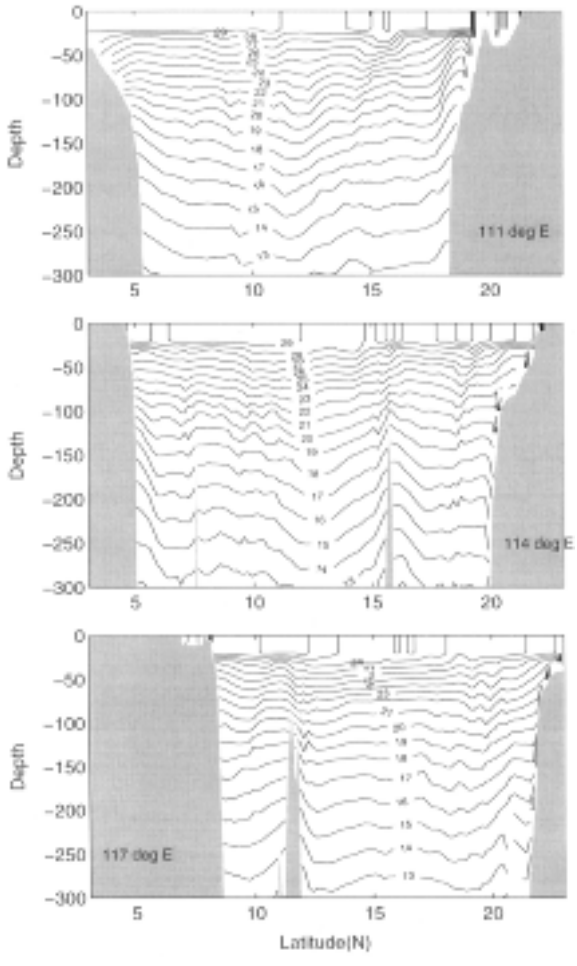

Fig. 10. CAOCS simulated mean temperature field during 14–25 May 1995 at several latitudinal cross section: (a) 111°E, (b) 114°E, and (c) 117°E.

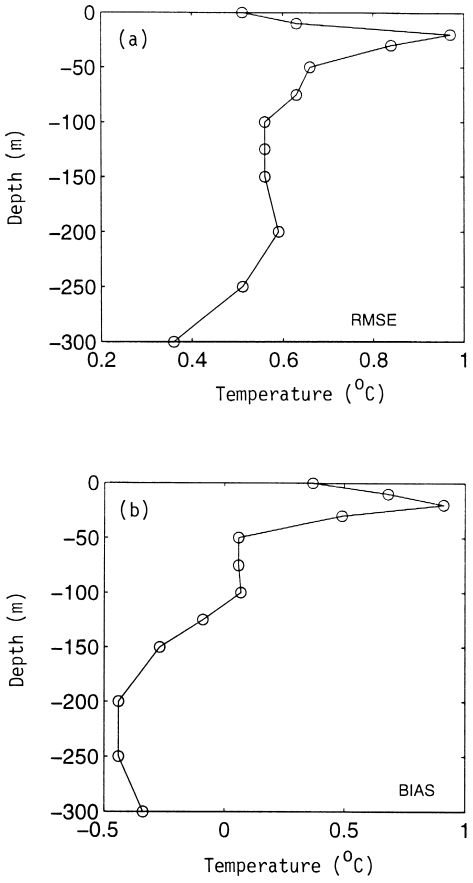

Fig. 11. Difference between CAOCS simulated and AXBT measured temperature fields: (a) *RMSE*, and (b) *BIAS*.

4.2 Velocity

4.2.1 Horizontal velocity fields

The simulated horizontal velocity field (Fig. 12) indicates the existence of a central SCS anticyclonic gyre surrounded by several cyclonic and anticyclonic eddies. Generally, the anticyclonic (cyclonic) eddies are associated with the warm (cool) pools. The kinetic features of these eddies are listed in Table 3. Furthermore, the magnitude of the velocities decreases with depth.

The simulated temperature and velocity fields indicate the existence of a central SCS warm-core anticyclonic eddy with several surrounding warm-core and cool-core eddies. Figure 13 shows the locations of these eddies at different depths.

4.2.2 Zonal cross sections of v-component

Four zonal cross-sections (19°N, 17°N, 13°N, and 7°N) of *v*-velocity show the vertical eddy structure (Fig. 14). Positive values indicate northward velocity, and negative values refer to southward velocity. Alternate positive and negative areas indicate the occurrence of cyclonic and anticyclonic eddies. At each zonal cross-section, neighboring eastern negative/western positive pattern refers to an anticyclonic eddy. And, neighboring western negative/eastern positive pattern refers to a cyclonic eddy.

The 19°N cross-section clearly shows the existence of the Bashi anticyclonic eddy near 117°E with the longitudinal span from 112°E to 121°E. The maximum *v*-velocity is around 15 cm/s. The 17°N cross-section clearly shows the existence of the central SCS anticyclonic eddy centered at

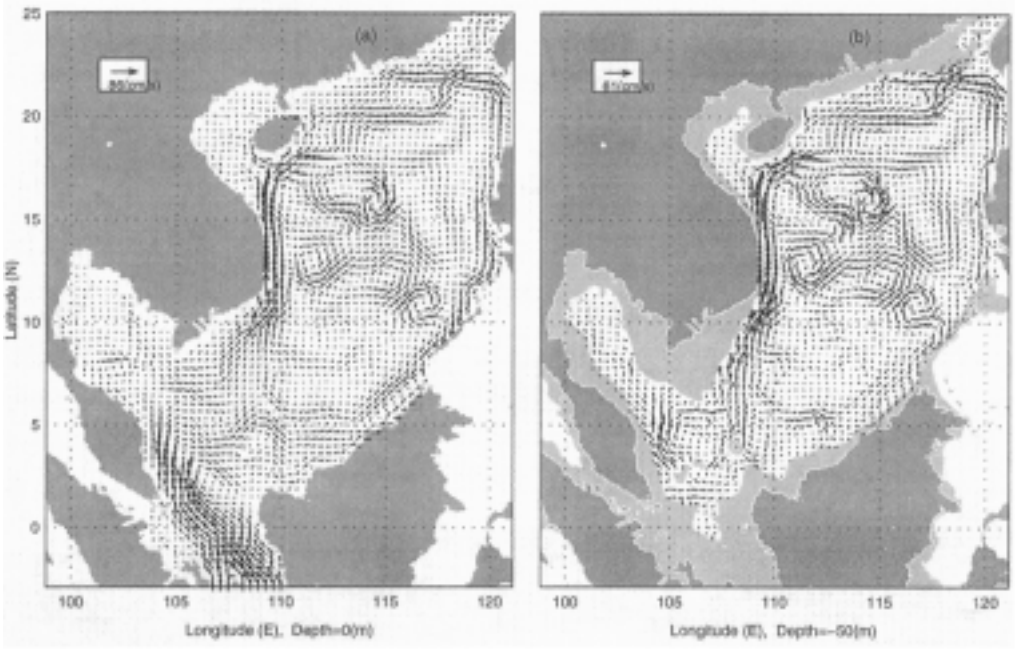

Fig. 12. CAOCS simulated mean horizontal velocity field during 14–25 May 1995 at different depths: (a) 0-m, (b) 50-m, (c) 100-m, (d) 200-m, and (e) 300-m.

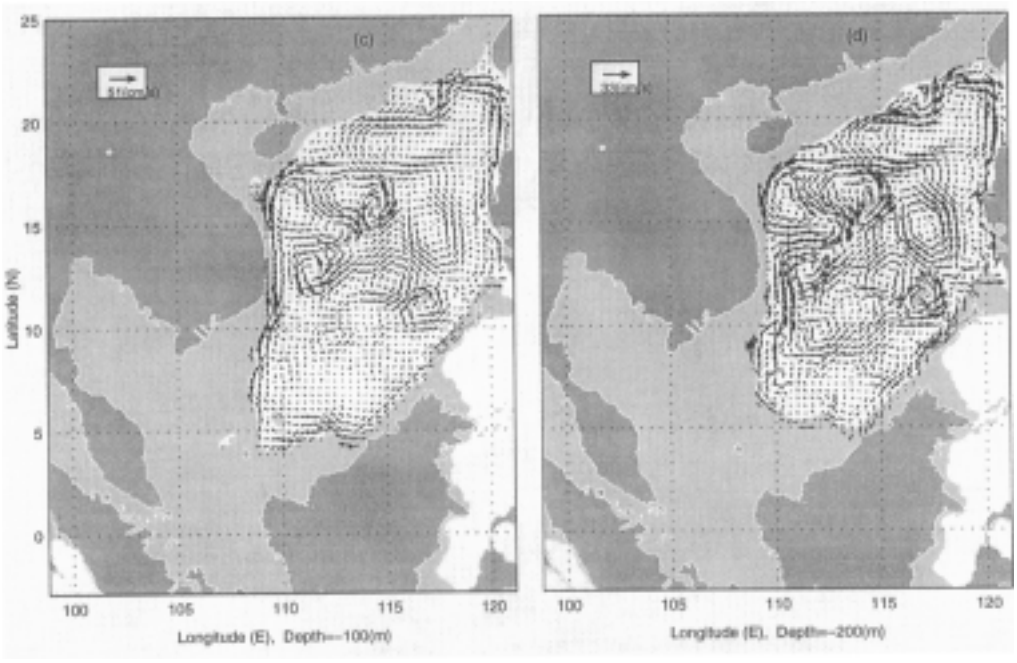

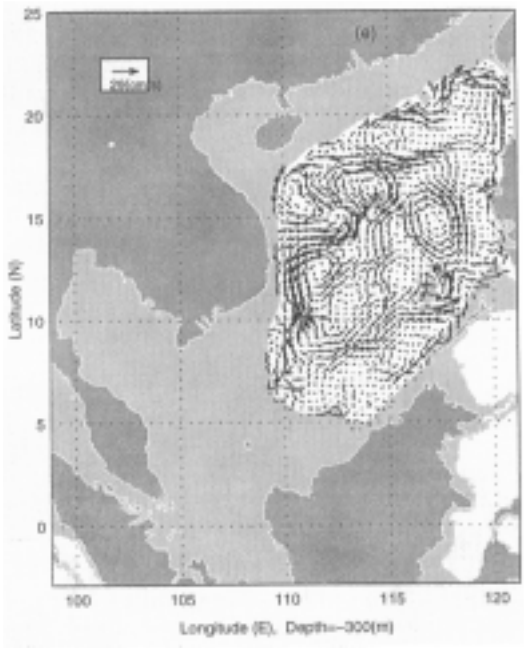

Fig. 12. (continued).

114°E. The zonal span of the central SCS eddy is around 500 km. The maximum *v*-velocity is around 20 cm/s. The 13°N cross-section clearly shows the existence of a double-eddy structure. Between 112°E and 118°E there is a strong anti-cyclonic eddy (the central SCS eddy) with a maximum *v*-velocity of 20 cm/s (appearing in the upper 50-m) and centered at 115°E. The zonal span of this eddy is around 600 km. This anticyclonic eddy is associated with the central SCS warm pool. To the west of the anticyclonic eddy, a cyclonic eddy appears between 111°E to 113°E. This cyclonic eddy is associated with the South Vietnam cool pool, and therefore, called the South Vietnam cool-core (cyclonic) eddy. The central SCS warm-core eddy and South Vietnam cool-core eddy share the same northward branch.

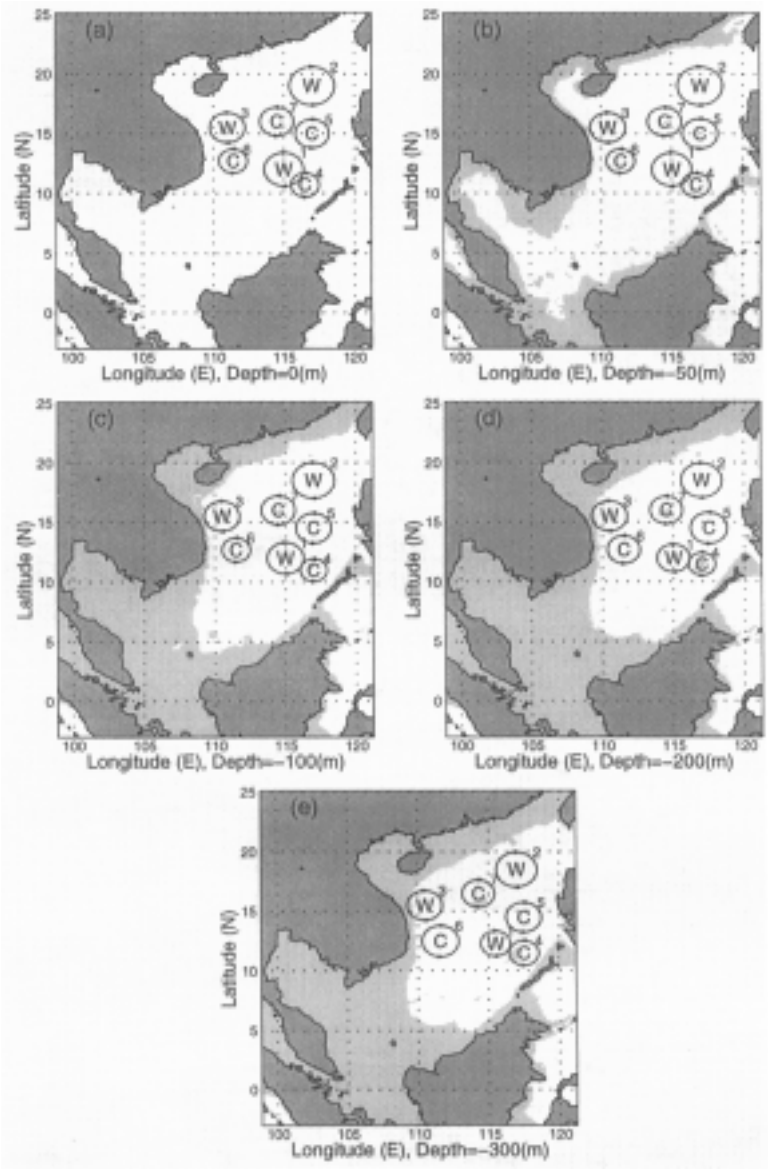

Fig. 13. Illustration of simulated South China Sea warm-core and cool-core eddies in May 1995 (1: Central SCS warm-core anticyclonic eddy, 2: Bashi warm-core anticyclonic eddy, 3: Xisha warm-core anticyclonic eddy, 4: Liyue cool-core cyclonic eddy, 5: Luzon cool-core cyclonic eddy, 6: South Vietnam cool-core cyclonic eddy, and 7: Zhongsha cool-core cyclonic eddy). Here, the circle of an eddy only shows the center location and the cyclonic or anticyclonic rotation, but does not show the size of the eddy.

4.2.3 Latitudinal cross sections of u-component

Three latitudinal cross-sections (111°E, 114°E, and 117°E) of *u*-velocity also show the vertical eddy structure (Fig. 15). Positive values indicate eastward velocity, and the negative values refer to westward velocity. Alternate positive and negative areas indicate the occurrence of cyclonic and anticyclonic eddies. At each latitudinal cross-section, neighboring southern negative/northern positive pattern refers to an anticyclonic eddy. However, neighboring northern negative/southern positive pattern refers to a cyclonic eddy.

The area with southern negative/northern positive *u*-pattern (anticyclonic eddy) coincides with the area of the downward bending isotherms (warm pool). At the 111°E cross-section, the central SCS warm-core eddy is recognized by an isotherm trough located at 12°N (Fig. 10), and an anticyclonic eddy is identified by the southern negative/northern positive *u*-pattern centered at 12°N (Fig. 15). At 114°E cross section, the central SCS warm-core eddy is recognized by an isotherm trough located at 13°N (Fig. 10), and an anticyclonic eddy is identified by the southern negative/northern positive *u*-pattern centered at 13°N (Fig. 15).

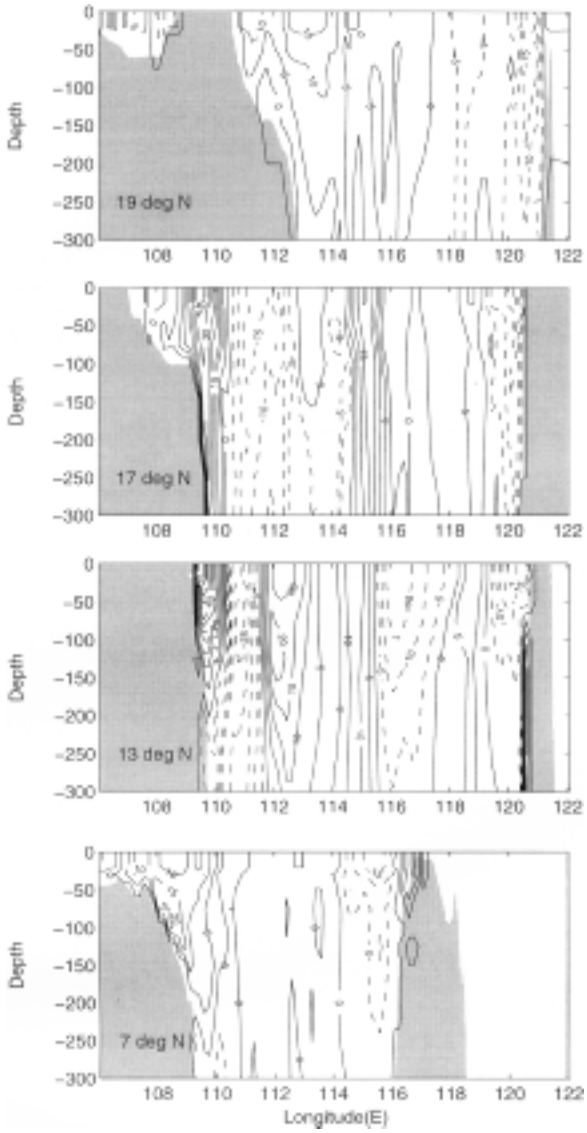

Fig. 14. CAOCS simulated mean velocity *v*-component in cm s^{-1} during 14–25 May 1995 at several zonal cross section: (a) 19°N, (b) 17°N, (c) 13°N, and (d) 7°N.

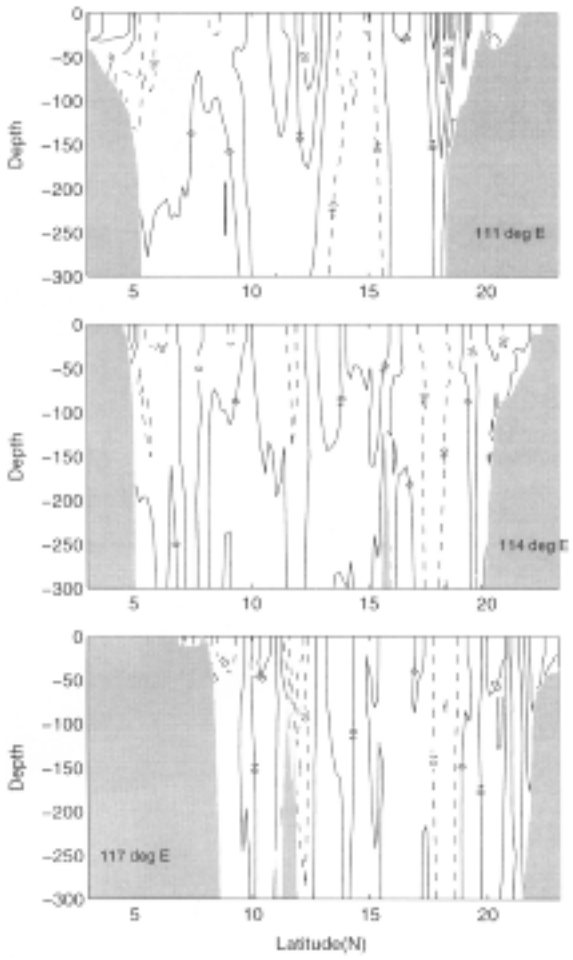

Fig. 15. CAOCS simulated mean velocity *u*-component in cm s^{-1} during 14–25 May 1995 at several latitudinal cross section: (a) 111°E, (b) 114°E, and (c) 117°E.

4.3 Comparison with earlier studies

This snapshot of the simulated multi-eddy structure agrees quite well with previous studies of individual SCS eddies appearing in mid-May. For example, the central SCS warm-core eddy was previously reported by the South China Sea Institute of Oceanology (SCSIO, 1985) and identified as a recurring phenomenon by analyzing historical data such as MOODS (Chu *et al.*, 1997a), NCEP monthly SST (Chu *et al.*, 1997b), and AXBT data (Chu *et al.*, 1998b). The surrounding smaller cool-core and warm-core eddies were identified separately by different authors (Dale, 1956; Uda and Nakao, 1974). Our contribution here is to present a model simulated multi-eddy structure in mid-May, the monsoon transition period.

5. Conclusions

(1) Comparing to the observational study on the AXBT measurement, the coastal atmosphere-ocean coupled system successfully simulates the South China Sea multi-eddy structure during 14–25 May 1995. These warm-core and cool-core eddies have radii varying from 100 km to 300 km and maximum tangential velocities ranging from 10 cm/s to 20 cm/s. The cool-core eddies are cyclonic and the warm-core eddies are anticyclonic.

(2) The simulated temperature and velocity fields show the existence of: a central SCS warm-core anticyclonic eddy with a maximum tangential velocity of 20 cm/s, strongest between the surface and 100-m depth, a Bashi warm-core anticyclonic eddy with a maximum tangential velocity of 20 cm/s, strongest between the surface and 100-m depth, a Xisha warm-core anticyclonic eddy with a maximum tangential velocity of 15 cm/s, strongest between the surface and 100-m depth, a South Vietnam cool-core

cyclonic eddy between surface and 100-m depth with a maximum tangential velocity of 20 cm/s at surface and decreasing with depth, a Liyue cool-core cyclonic eddy with a maximum tangential velocity of 20 cm/s, strongest between the surface and 50-m depth, and a Zhongsha cool-core cyclonic eddy with a maximum tangential velocity of 16 cm/s, the weakest of the cool-core eddies.

(3) The RMS error between simulated and observed temperature fields is around 0.5°C at the surface, within 0.36° to 0.62°C below 50 m depth, and 0.95°C at 30 m depth. The overall RMS error is around 0.6°C. The inaccuracy is partially due to the low vertical resolution of the POM model in the SCS deep basin.

Acknowledgements

The authors wish to thank George Mellor and Tal Ezer of the Princeton University for most kindly providing them with a copy of the POM code, and to appreciate Filippo Giorgi, Gary Bates, and Christine Brodeur of the National Center for Atmospheric Research for allowing them to use the RegCM2. This work was funded by the Office of Naval Research NOMP Program, the Naval Oceanographic Office, and the Naval Postgraduate School.

References

Anthes, R. A., E. Y. Hsie and Y. H. Kuo (1987): Description of the Penn State/NCAR Mesoscale Model Version 4 (MM4). NCAR Tech. Note, NCAR/TN-282+STR, 66 pp.

Blumberg, A. and G. Mellor (1987): A description of a three dimensional coastal ocean circulation model. p. 1–16. In *Three-Dimensional Coastal Ocean Models*, ed. by N. S. Heaps, American Geophysics Union, Washington, D.C.

Briegleb, B. P. (1992): Longwave band model for thermal radiation in climate studies. *J. Geophys. Res.*, **97**, 7603–7612.

Chu, P. C. and C. P. Chang (1997): South China Sea warm pool in boreal spring. *Adv. Atmos. Sci.*, **14**, 195–206.

Chu, P. C., H. C. Tseng, C. P. Chang and J. M. Chen (1997a): South China Sea warm pool detected in spring from the Navy's Master Oceanographic Observational Data Set (MOODS). *J. Geophys. Res.*, **102**, 15761–15771.

Chu, P. C., S. H. Lu and Y. C. Chen (1997b): Temporal and spatial variabilities of the South China Sea surface temperature anomaly. *J. Geophys. Res.*, **102**, 20937–20955.

Chu, P. C., C. Fan, C. J. Lozano and J. L. Kerling (1998a): An airborne expandable bathythermograph survey of the South China Sea, May 1995. *J. Geophys. Res.*, **103**, 21637–21652.

Chu, P. C., C. W. Fan and W. J. Cai (1998b): Evaluation of P-vector method using modular ocean model (MOM). *J. Oceanogr.*, **54**, 185–198.

Chu, P. C., Y. C. Chen and S. H. Lu (1998c): Wind-driven South China Sea deep basin warm-core/cool-core eddies. *J. Oceanogr.*, **54**, 347–360.

Dale, W. L. (1956): Winds and drift currents in the South China Sea. *Malay. J. Trop. Geogr.*, **8**, 1–31.

Dickinson, R. E., A. Henderson-Sellers and P. J. Kennedy (1993): Biosphere-Atmosphere Transfer Scheme (BATS) version 1E as coupled to the NCAR Community Climate Model. NCAR Tech. Note, NCAR/TN-387+STR, 72 pp.

Giorgi, F. and G. T. Bates (1989): The climatological skill of a regional model over complex terrain. *Mon. Wea. Rev.*, **117**, 2325–2347.

Giorgi, F., M. R. Marinucci and G. T. Bates (1993a): Development of a second-generation regional climate model (RegCM2). Part I: Boundary-layer and radiative transfer processes. *Mon. Wea. Rev.*, **121**, 2749–2813.

Giorgi, F., G. De Canio and G. T. Bates (1993b): Development of a second-generation regional climate model (RegCM2). Part II: Convective processes and assimilation of lateral boundary conditions. *Mon. Wea. Rev.*, **121**, 2814–2832.

Grell, G. A. (1993): Prognostic evaluation of assumptions used by cumulus parameterization. *Mon. Wea. Rev.*, **118**, 1561–1575.

Haney, R. L. (1971): Surface boundary conditions for ocean circulation models. *J. Phys. Oceanogr.*, **1**, 241–248.

Holtslag, A. A. M., E. I. F. de Bruijin and H. L. Pan (1990): A high resolution air mass transformation model for short-range weather forecasting. *Mon. Wea. Rev.*, **118**, 1561–1575.

Hsie, E. Y., R. A. Anthes and D. Keyser (1984): Numerical simulation of frontogenesis in a moist atmosphere. *J. Atmos. Sci.*, **41**, 2581–2594.

Hu, J. and M. Liu (1992): The current structure during summer in southern Taiwan Strait. *Tropic Oceanol.*, **11**, 42–47 (in Chinese).

Huang, Q. and W. Wang (1994): Current characteristics of the South China Sea. p. 39–46. In *Oceanology of China Seas*, ed. by Z. Di, L. Yuan-Bo and Z. Cheng-Kui, Kluwer, Boston.

Kuo, H. L. (1974): Further studies of the parameterization of the influence of cumulus convection on large-scale flow. *J. Atmos. Sci.*, **31**, 1232–1240.

Levitus, S. (1984): Climatological atlas of the world ocean. NOAA Professional Paper, 13, U.S. Government Printing Office, Washington, D.C., 173 pp.

Nitani, H. (1970): Oceanographic conditions in the sea east of Philippines and Lozon Strait in summer of 1965 and 1966. p. 213–232. In *The Kuroshio—A Symposium on Japan Current*, ed. by J. D. Mar, East-West Press, Honolulu.

SCSIO (1985): *Integrated Investigation Report on Sea Area of the South China Sea*, Vol. 2, pp. 183–231, Science Press, Beijing (in Chinese).

SCSMEX Science Working Group (1995): The South China Sea Monsoon Experiment (SCSMEX) Science Plan. NASA/ Goddard Space Flight Center, Greenbelt, 65 pp.

Smagorinsky, J. (1963): General circulation experiments with the primitive equations, I. The basic experiment. *Mon. Wea. Rev.*, **91**, 99–164.

Soong, Y. S., J. H. Hu, C. R. Ho and P. P. Niiler (1995): Cold-core eddy detected in South China Sea. *EOS Trans., AGU*, **76**, 345–347.

Uda, M. and T. Nakao (1974): Water masses and currents in the South China Sea and their seasonal changes. *The Kuroshio—Proceedings of the 3rd CSK Symposium*, Bangkok, Thailand, 161–188.

Wyrtki, K. (1961): Scientific results of marine investigations of the South China Sea and the Gulf of Thailand 1959–1961. Naga Report, Vol. 2.